Electron and ion heating in a high-voltage toroidal theta pinch with parallel or antiparallel bias fields

R. L. Merlino,[a] G. C. Goldenbaum, C. Chin-Fatt, Y. P. Chong, A. W. DeSilva, H. R. Griem, R. A. Hess, and D. P. Murphy[b]

Department of Physics and Astronomy, University of Maryland, College Park, Maryland 20742
(Received 22 April 1981; accepted 24 September 1981)

Rapid heating of electrons and ions has been observed in a high-voltage toroidal theta pinch with initial bias fields either parallel or antiparallel to the fast rising toroidal field. The elimination of rapid end losses has permitted higher electron temperatures to be attained. In contrast to the results of linear theta pinches in which $T_e \lesssim 0.3\ T_i$, it is now found that $T_e \simeq T_i$. The ion heating is similar to that observed in the linear case indicating that the effective microinstability heating process is maintained in a toroidal system. Higher temperatures were observed with antiparallel bias fields, but in both cases superthermal electron populations were observed indicating that the turbulent heating process involves electron tail formation.

I. INTRODUCTION

For nearly twenty-five years, researchers have produced high-temperature plasmas in linear theta pinch devices.[1] Typically, this is accomplished by applying a rapidly rising magnetic field along the axis of a low-inductance, single-turn coil containing pre-ionized deuterium at an initially low pressure (1–50 mTorr). If the magnetic field rise time is sufficiently fast ($\lesssim 1$ μsec), the plasma implodes toward the axis of the system and a magnetic shock structure[2] is formed. Using this technique, shock velocities corresponding to ion energies of several thousand electron volts can be achieved with electrical efficiencies as high as 5% (stored energy into plasma energy). Ions upstream of the shock may be reflected by the electrostatic potential associated with the imploding magnetic piston acquiring twice the piston velocity,[3] as evidenced by the neutron emission resulting from D-D fusion reactions[4,5] and by turbulence generated by their interaction with the ambient plasma.[6] The directed ion energy may eventually thermalize on time scales faster than ordinary binary collision times, leading to thermonuclear plasmas. The continuing interest in theta pinches is attributable, in large part, to this high efficiency in ion heating, as well as its geometric simplicity. Indeed, some of the proposed "alternate concept" field reversed pinches[7] and spheromak[8] fusion devices are based largely on the theta pinch configuration.

Electron temperatures in linear theta pinches tend to be below average ion temperatures. Electron energy transport along the open field lines, which is more rapid for electrons than ions, is thought to be a decisive energy loss mechanism during the implosion phase. The University of Maryland high voltage, toroidal theta pinch, "Thor," was designed to study implosion heating in the absence of thermal end losses. An important question which this experiment addresses is whether or not the ion heating processes remain as effective in a toroidal system where electron temperatures may be higher than those in corresponding linear devices.

A significant aspect of many theta pinch experiments is that for low to moderate density plasmas (10^{12} cm^{-3} $\lesssim n_{e0} \lesssim 10^{14}$ cm^{-3}) and rapidly rising magnetic pulses ($dB/dt \gtrsim 10^{10}$ G sec^{-1}) ordinary binary collision processes occur on time scales longer than the experimental time and various microinstability processes[9] appear to be responsible for the observed plasma heating and dynamics. These microinstability processes are driven either by the free energy available in the relative azimuthal drift between electrons and ions in the current sheath, $V_d = V_{e\theta} - V_{i\theta} = (c/4\pi ne)(\partial B_z/\partial r)$, which is associated with the radial gradient in the axial magnetic field B_z, or other drifts associated with temperature and density gradients. Depending on the value of the drift velocity, various cross-field instabilities (e.g., Buneman two-stream, ion-acoustic, and lower-hybrid drift) may grow unstable at any time or position in the plasma where the necessary conditions are present. These instabilities produce turbulent field fluctuations which are manifested macroscopically as an anomalous resistivity leading to a reduction in the drift velocity and a corresponding anomalous Joule heating of electrons and ions in the current sheath.

Analytical calculations[10] show that the turbulent heating of electrons is at least comparable to that of the ions. The relatively low electron temperatures observed in various linear theta pinch experiments[4,5,11,12] are, therefore, presumably due to rapid electron end losses. Numerical computations by Caponi and Krall[13] have shown that heat loss by conduction along open field lines is indeed a viable mechanism for limiting electron temperatures on the implosion timescale. However, turbulence may affect not only the plasma resistivity, but thermal conduction as well. Chodura *et al.*[5] showed that the electron temperature measured in the Garching high-voltage theta pinch is due to enhanced resistivity in the shock and is an indication of nonclassical heat conduction parallel to the magnetic field. Their simulation results indicated that axial heat flow is reduced over classical heat flow when the effects of turbulence are included.

In addition to end loss, the results of linear theta pinch experiments revealed that other effects, notably initial bias fields, play an important role in plasma

[a] Present address: Department of Physics and Astronomy, University of Iowa, Iowa City, Iowa 52242.
[b] Present address: JAYCOR, Alexandria, Virginia 22304.

 0031-9171/81/122358-14$00.90

heating. Experiments on the Maryland fast theta pinch[4] showed quite different behavior depending on the direction of the initial bias field relative to the main implosion field. In the antiparallel mode, a magnetic piston is quickly formed which reflects ions in a beam moving at twice the piston velocity.[14,15] X-ray emission corresponding to electron energies of approximately 2 keV was observed which originated near the field reversal point.[16] The parallel bias mode is characterized by a very rapid diffusive penetration of the magnetic field through over half the plasma volume, which is consistent with an instability-enhanced resistivity much larger than the classical Spitzer resistivity. Furthermore, very little electron heating is observed with parallel bias fields as evidenced by the lack of x-ray emission. In the antiparallel mode, spectroscopic data[17] indicated that the plasma beyond the ends of the coil was being heated too rapidly to be explained by classical energy transport. This result coupled with later observations of closed magnetic field lines in the end regions[18] indicates enhanced electron energy transport across the field lines presumably due to turbulence. However, spatially resolved neutron emission measurements[19] indicated better confinement of ions with antiparallel bias fields than with parallel fields.

The investigation of plasma heating in the Maryland toroidal device was performed in deuterium plasmas at an initial density of approximately 10^{14} cm^{-3} and initial bias fields less than or equal to 1 kG either antiparallel (case 1) or parallel (case 2) to the main implosion field. Thus, direct comparisons of heating results are obtained for different initial bias conditions in an experiment in which rapid end losses are eliminated.

The results of our preliminary plasma heating experiments in Thor have been reported elsewhere.[20] These preliminary investigations were carried out in an acrylic vacuum vessel at lower initial densities (about 10^{13} cm^{-3}) and smaller antiparallel bias fields (less than or equal to 100 G) than the experiments now described. At a compressed deuterium density of approximately 1×10^{14} cm^{-3}, the observed neutron yield corresponded to $kT_i = 3.5$ keV for a fully Maxwellian plasma. Spatially averaged relative x-ray intensities indicated an electron temperature of 7 keV with absolute intensities consistent with calculations also allowing for bremsstrahlung on 5% of (carbon) impurities. Magnetic probe measurements revealed a 5–10 cm wide magnetic piston corresponding to $(1-2)c/\omega_{pi}$ at $n = 0.5\times10^{14}$ cm^{-3}, and propagating inward at about 10^7 cm/sec. The resulting high-β plasma region remained macroscopically stable in the outer half of the torus for about 2 μsec, although the toroidal shift was large and only arrested at the wall (no vertical field was provided). In contrast to similar theta pinches, these experiments showed that higher electron temperatures could be attained when electron energy losses along open field lines are eliminated and that the microinstability heating processes remain effective in going from $T_e/T_i \lesssim 0.3$ to $T_e/T_i \gtrsim 2$.

The electron heating results reported in this investigation were obtained from an analysis of plasma x-ray emission and spatially resolved x-ray emission from an aluminum target in the plasma. Electron temperatures are determined from x-ray filter transmission ratios and the density of heated electrons is estimated from absolute x-ray intensities using calibrated detectors. Plasma dynamics and sheath structure are determined from an analysis of magnetic probe signals. Ion heating is inferred from neutron yield measurements and spectroscopic observations of impurity lines in the plasma.

A complete description of the toroidal theta pinch is given in Sec. II followed by a brief discussion of the diagnostic methods in Sec. III. The results of the heating measurements for the antiparallel and parallel bias configurations are presented in Sec. IV. In Sec. V the results are discussed and compared with prediction of microinstability heating theories. Conclusions and summary are given in Sec. VI.

II. EXPERIMENTAL APPARATUS

A. Vacuum system and field coils

The toroidal theta pinch, "Thor," consists of a fused silica torus of 50 cm major radius and 20 cm minor radius surrounded by a one-turn, cast aluminum field coil (Fig. 1). Evacuation is achieved through six equally spaced pump ports (approximately 5 cm in diameter by 8 cm high) including an elongated diagnostic port which allows better diagnostic access. Using a turbomolecular pump, a base pressure of 5×10^{-6} Torr is achieved. The toroidal theta pinch coil is divided into six separate 60° segments surrounding the torus. Bias and preheating capacitor banks are connected to the coils using coaxial cables. Six oil-immersed, high-voltage pulsers are connected to the coil in parallel using insulated copper strip lines. The silica torus and coil structure are immersed in a weak aluminum chloride water solution to grade the high electrical stresses that appear on the edges of the conductors.

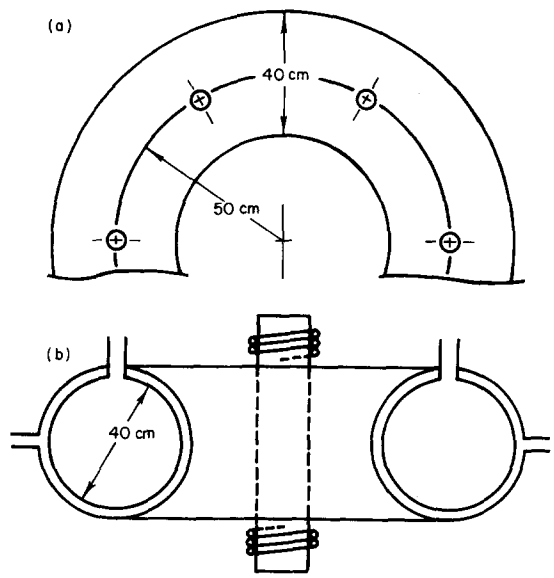

FIG. 1. Schematic of toroidal vacuum vessel and theta pinch coil. (a) Top view; (b) cross sectional view showing diagnostic ports and toroidal current transformer.

B. Breakdown, preheating, and toroidal current generation

Breakdown and preheating of the deuterium fill gas (1–2 mTorr) is achieved by discharging capacitors (12 μF, 9.6 kJ) in parallel through the theta pinch coils, and by a low-energy capacitor discharge (0.2 μF, 15 J) into two spark plugs located at opposite pump ports. The sparkers provide a few electrons which initiate the pre-ionization process which is completed by the ringing preheater discharge through the theta pinch coils. The bias bank (4800 μF, 60 kJ) is fired first, generating a quasi-static toroidal field less than or equal to 1 kG with variable polarity relative to the fast rising implosion field.

Toroidal currents are induced in the preheated plasma to slow the outward toroidal shift of the initial plasma. This is accomplished by a capacitor discharge (800 μF, 1.6 kJ) into an air-core inductor on the axis of symmetry [Fig. 1(b)]. Additional toroidal currents may be generated using the theta pinch coils as the primary of a one-turn transformer with the plasma as secondary, and fed by a capacitor bank (15 μF, 1.7 kJ) at one toroidal location. The peak poloidal field resulting from these plasma currents ($\lesssim 20$ kA) is less than or equal to 200 G at the time when the main bank is fired.

C. High-voltage generators

Shock heating in Thor is carried out using a hexagonal array of high power ($\lesssim 10^{12}$ W), low inductance, synchronized pulser modules. Details of the design and operation of these high voltage "LC" generators have been given elsewhere.[21] These compact, low inductance ($\lesssim 350$ nH) pulsers can produce a peak open circuit voltage of 580 kV. In the experiments described here the pulsers were operated at about half the peak design voltage resulting in a peripheral poloidal voltage of approximately 140 kV around the theta pinch coil. The six pulser modules deliver a sinusoidal current pulse to the load coil (52 nH) with a peak current of 1.5 MA rising in 1 μsec which produces an 8 kG toroidal magnetic field at the inner wall at the typical operating voltage. This current is crowbarred at 1.2 μsec from its initiation and then decays with an L/R time constant of about 20 μsec. The complete theta pinch electrical circuit is shown in Fig. 2, and a summary of the machine parameters is given in Table I.

D. Initial plasma parameters

The initial toroidal bias field (B_{t0}) and vertical component of the poloidal field (B_{v0}) were measured using a pair of multi-turn magnetic probes. The initial density (n_{e0}) was measured using a helium neon interferometer and a double Langmuir probe. The spatially resolved electric probe results showed an approximately Gaussian density profile centered at $R \simeq 55$ cm with a FWHM of about 12–15 cm. The peak electron density inferred from interferometry was $n_{e0} \simeq (2-3)\times 10^{14}$ cm^{-3}. A summary of these initial plasma parameters at the time of application of the high-voltage pulse (i.e., $t=0$) is given in Table II. These values correspond to $R = 55$ cm and approximately the horizontal midplane.

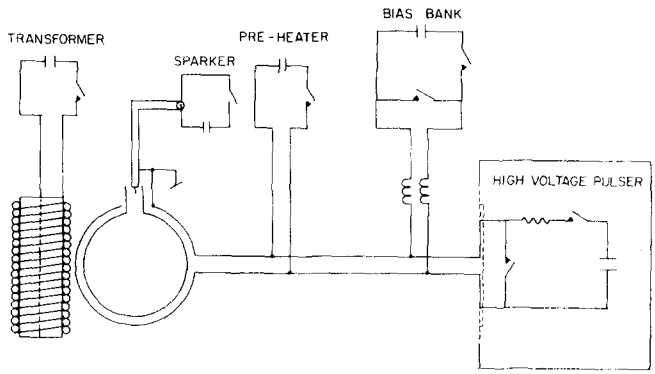

FIG. 2. Electrical schematic of complete theta pinch circuit.

III. DIAGNOSTICS

A. Magnetic field measurements

A set of three movable probe coils was used to map the toroidal field along the major radius in approximately the horizontal midplane. The probes consist of

TABLE I. Toroidal theta pinch parameters.

A.	Vacuum vessel:	
	Fused quartz	
	Major radius:	50 cm
	Minor radius:	20 cm
B.	Coil:	
	Cast aluminum, in six 60° segments	
	Total inductance	52 nH
C.	Bias bank:	
	Field:	0–1 kG
	Capacitance:	4800 μF
	Energy:	60 kJ
D.	Pre-heater:	
	Capacitance:	12 μF
	Voltage:	30 kV
	Period:	17 μsec, not crowbarred
	Energy:	10 kJ
E.	Toroidal current drivers:	
	(1) Capacitance:	800 μF
	Inductance:	10 μH
	Period:	550 μsec
	(2) Capacitance:	15 μF
	Inductance:	1 μH
	Period:	24 μsec
F.	High-voltage generators:	
	Six, 7-stage swinging LC generators	
	Total energy[a]:	600 kJ
	Peak open circuit voltage[a]:	500 kV
	Peak field[a]:	12 kG
	1/4 period:	0.9 μsec
	Crowbar L/R time:	20 μsec
	Poloidal electric field[a]:	4 kV/cm
	Total internal inductance:	58 nH

[a]At full design voltage, typical operation at (1/2) maximum design voltage.

TABLE II. Initial plasma parameters.

	Antiparallel bias (↑↓)	Parallel bias (↑↑)
n_{e0}	2×10^{14} cm^{-3}	3×10^{14} cm^{-3}
B_{T0}	−900 G	+850 G
B_{V0}	100 G	200 G

two turns of No. 40 enameled wire wound on a MACOR form of 4 mm diameter and attached to a small piece of copper tubing. The probes are center-tapped and connected to wideband (0.01–50 MHz) impedance matching transformers in an electrically balanced configuration to minimize electrostatic pickup. The probes are coated with a refractory material (Sauereisen) reinforced with fiberglass particles to provide electrical and thermal isolation from the plasma. The probe signals are passively integrated and recorded on transient digitizers for subsequent analysis and display. Due to the low frequency cutoff of the transformers, the probes are sensitive only to the change in the toroidal field, ΔB_t, produced by the fast magnetic compression. The ambient bias field, $B_{t0}(R)$, is added to the main compression field, $\Delta B_t(R)$, giving the net toroidal magnetic field $B_t(R) = B_{t0}(R) + \Delta B_t(R)$. The results of the magnetic field measurements will be presented in Sec. IV.

B. Ion heating measurements

Neutron yields and Doppler broadening measurements of impurity spectral lines have been used as diagnostics to determine the ion temperature. A plastic scintillator-photomultiplier detector was used which was calibrated so that the pulse area could be directly related to neutron yields. The neutron yield N_{DD} is related to the fusion reaction rate $\langle\sigma v\rangle_{DD}$ by $N_{DD} \approx \frac{1}{2} n_D^2 \times \langle\sigma v\rangle_{DD}(\Delta t)V$, where n_D is the deuterium ion density, Δt is the duration of the neutron emission, and V is the volume of neutron emitting plasma. The deuterium density and emission volume are determined from line density measurements along various chords in the plasma using a helium-neon interferometer and line-of-sight estimates from the magnetic field profiles. The reaction rates $\langle\sigma v\rangle_{obs}$ determined from the neutron yield are compared to theoretical rates[22] (for an assumed ion distribution) to determine the deuterium ion temperature. Further information on ion heating was obtained from spectroscopic observations on lines of impurity ions.

C. Electron heating measurements

Electron heating in Thor was studied by observing the plasma x-ray emission and x-ray emission from movable targets in the plasma. The electron temperature was derived from relative x-ray intensities[23] and the density of heated electrons was estimated from absolute x-ray intensities. Scintillator-photomultiplier detectors were used in conjunction with thin absorber foils (beryllium or aluminum) which provided spectral sensitivity. The energy received by one such scintillator detector, and accordingly also the photomultiplier signal, is determined by

$$F_1 = C \int_0^\infty \exp[-\mu_1(E)d_1]\{1 - \exp[-\mu_s(E)d_s]\} I(E)dE , \quad (1)$$

where E is the x-ray energy, $\mu_1(E)$ is the x-ray mass absorption coefficient of the filter, d_1 is the filter thickness, $\mu_s(E)$ is the scintillator energy absorption coefficient, d_s is the scintillator thickness, and C is a constant depending on the geometry of the detection system. The function $I(E)$ is the spectral distribution of x-ray intensity incident upon the filter.

Plasma x-ray emission, $I_p(E)$, is determined primarily by the bremsstrahlung radiation and recombination radiation due to impurities, both of which have essentially the same spectral distribution given by

$$I_p(E) \propto \exp(-E/kT_e), \quad (2)$$

where T_e is the Maxwellian electron temperature. For the plasma parameters discussed in this paper, line radiation from partially ionized impurity species was either unimportant or occurred near the low energy cutoff of the filters and was therefore highly attenuated.

The spectral distribution of target bremsstrahlung radiation from plasma electrons has been derived by Adlam and Taylor.[24] This diagnostic technique has been applied in a number of turbulent heating experiments[16,25-27] to determine the temperature and density of heated electrons. The spectral distribution of the continuum target emission, I_t, is given by

$$I_t(E) \propto (E/kT_e + 2)\exp(-E/kT_e) \quad (3)$$

for a Maxwellian electron distribution. The deduction of this formula is based upon: (i) the formation of plasma sheaths at the plasma-target boundary, and (ii) the continuum x-ray spectrum produced when monoenergetic electrons strike a thick target.[28] By balancing the ion and electron current to the target (the target is at the plasma floating potential) the total energy radiated per cm^2 of target surface, per second, per steradian can be shown to be proportional to $n_e T_e^{5/2}$.

The apparatus used for detecting the plasma and target x-ray emission is shown schematically in Fig. 3. For plasma x-ray measurements the target is removed and beryllium filters (12.5 and 50 μm) are inserted in the detector. This system is most sensitive for soft x rays produced by electrons with temperatures in the range of 0.1–1.0 keV. The target x-ray measurements are carried out using an aluminum target (2.5 cm diameter × 0.16 cm thick), supported by a thin (0.16 cm) stainless steel rod which is attached to the detector assembly as shown in Fig. 4. The lead aperture limits the field of view of the detector (two channels are used simultaneously) to a single spot on the target. The target-detector system is placed in one of the pump ports through a vacuum seal arrangement which allows the entire system to be rotated to any radial position in the horizontal midplane in order to obtain spatial resolution. Aluminum filters (25 and 250 μm) are used to estimate the electron temperature by comparing the experimental intensity ratios to those computed by ap-

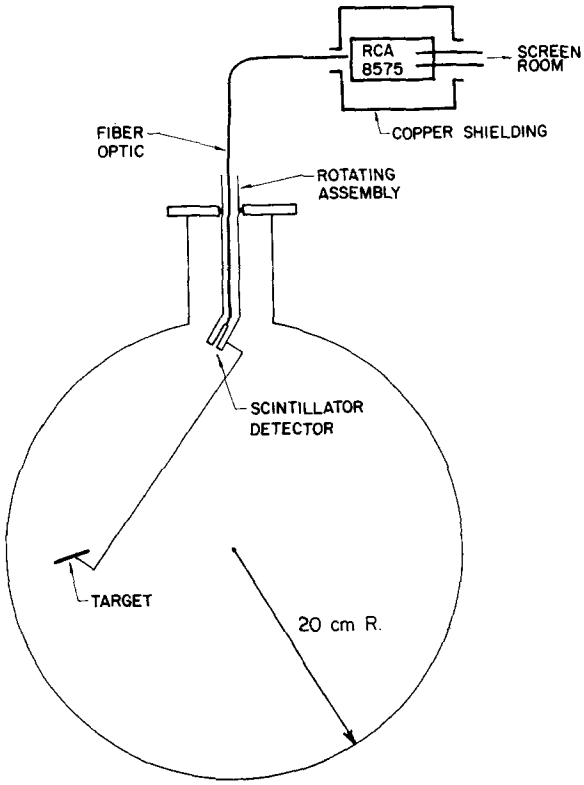

FIG. 3. Experimental apparatus used for plasma and target x-ray measurements.

plying Eq. (1) for different filter thicknesses. The numerical calculation includes an energy dependent scintillator absorption, since the (Pilot B plastic) scintillator absorption thickness is optimized to give measurable signals while reducing the detection sensitivity for hard x rays and neutrons. The detectors are first calibrated relative to each other by inserting identical filters in each channel and recording photomultiplier signals from many plasma shots.

The density of heated electrons may be estimated from the absolute x-ray intensity and the electron temperature results. The detector calibration (depending on scintillator efficiency, fiber optic light collection efficiency, and cathode quantum efficiency) was determined using a pulsed (100 nsec) monochromatic (Cu K_α) x-ray source at the National Bureau of Standards.[29] For the case of target x-ray emission the contribution from characteristic aluminum radiation was estimated, using measured K_α yields,[30] and was found to be negligible for the electron energies encountered in this experiment and for the filters used in the detection system. We should point out that while all of the above analysis

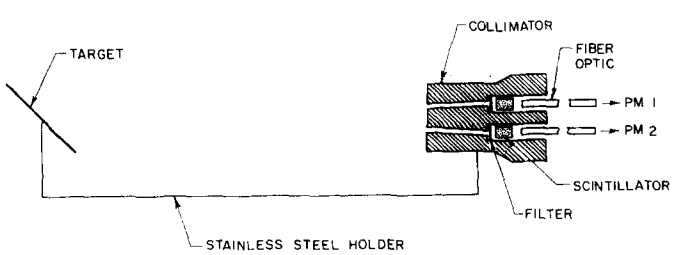

FIG. 4. Details of the plasma/target x-ray detection system (collimator-scintillator arrangement).

has assumed a Maxwellian electron distribution, the intensity ratios are rather insensitive to the exact details of the electron distribution. Jancarik and Snowden have demonstrated[31] that even if the electron distribution varies considerably from a Maxwellian, the temperature based on the procedure outlined here is a good estimate of the average electron energy. It is also possible, in some cases, to estimate the shape of the electron distribution by choosing filter materials with different absorption edges.

The most definitive measurement of the electron temperature is Thomson scattering of ruby laser light. However, the application of high voltages in this experiment (less than or equal to 300 kV) imposed severe restrictions on radial access ports due to the requirements of electrical insulation. (Recall that the torus and coil are immersed in a liquid solution.) Thus, without radial (side) access ports, 90° Thomson scattering was prohibited.

IV. EXPERIMENTAL RESULTS

A. Magnetic field profiles

1. *Antiparallel bias (↑↓)*

The toroidal magnetic field profiles for times up to 1 μsec after initiation of the main bank current are shown in Fig. 5(a). (These profiles include the initial bias field.) During the implosion, a magnetic piston structure is formed which propagates toward the magnetic axis at an average speed of approximately 1.3×10^7 cm/sec. The piston steepens as it encounters the bulk of the initial density distribution. After 1 μsec the implosion begins to slow down [Fig. 5(b)], reaching peak compression at about 1.2 μsec resulting in a compressed density of 2×10^{15} cm^{-3} and a compressed initial bias field of −2 kG in the center of the density distribution.

During the implosion, the sheath width (i.e., the width of the transition region between plasma and external magnetic field) corresponds to $(2-4)(c/\omega_{pi})$ at $n_e = 5\times10^{14}$ cm^{-3} (average sheath density). The measured sheath width ΔL is determined as the distance between the radial positions, where the magnetic field reaches roughly 90% of its minimum and maximum value. This rather wide ($\gg c/\omega_{pe}$) magnetic sheath is an indication of microinstability enhanced resistivity in the sheath region driven by the cross-field poloidal currents. After the implosion has slowed down, the resistivity can be estimated using the equation describing magnetic diffusion in a rigid conductor, i.e.,

$$\nabla^2 \mathbf{B} = \frac{4\pi}{\eta c^2}\frac{\partial \mathbf{B}}{\partial t} . \tag{4}$$

For typical implosion values, we get $\eta'' \approx 4\pi(\Delta L)^2/c^2 t \approx 10^{-12} - 10^{-13}$ sec, which is about a factor of 10^3 times the transverse Spitzer–Härm resistivity. From the magnetic field profiles and density in the sheath it is possible to estimate the drift velocity $\mathbf{V}_d = \mathbf{V}_i - \mathbf{V}_e$ corresponding to the poloidal currents using Ampere's law in the form

$$\nabla \times \mathbf{B} = (4\pi/c) n_e \mathbf{V}_d . \tag{5}$$

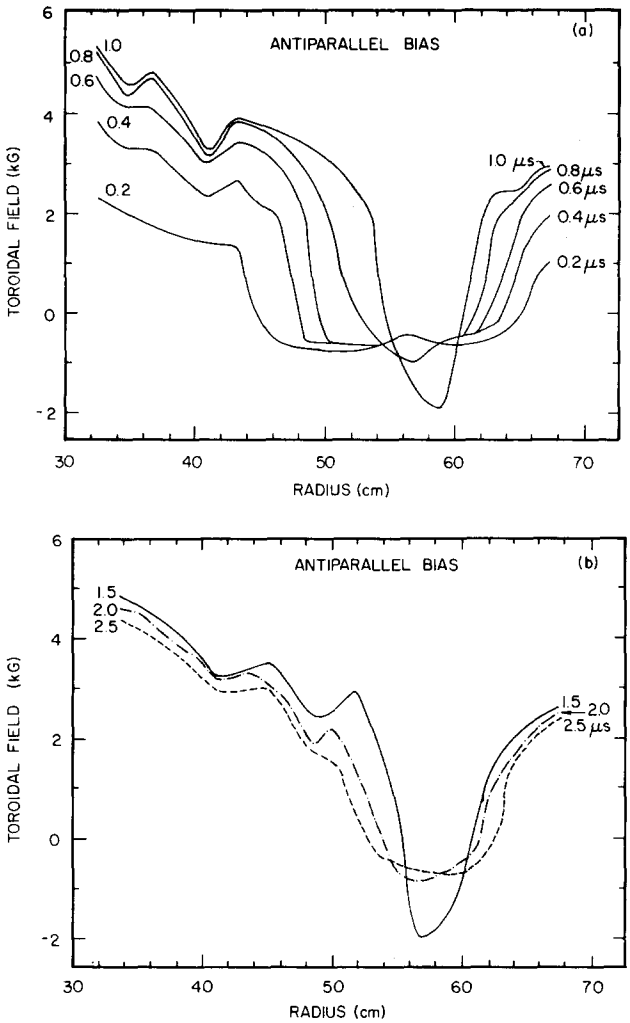

FIG. 5. Toroidal magnetic field profiles for the antiparallel bias case: (a) profiles for 0.2 μsec to 1.0 μsec, (b) profiles at 1.5, 2.0, and 2.5 μsec.

The time history of this drift velocity, for the antiparallel case, is shown as the solid curve in Fig. 6. This drift velocity is initially quite high ($\sim 8\times10^7$ cm/sec) due to the high induced electric field (≈ 1 kV/cm) applied to the tenuous outer region of plasma. Since this relative drift energy is available to drive various microinstabilities, it is important to note that for times less than about 0.2 μsec $V_d > v_e$ (electron thermal velocity), and decreases to a value such that $v_e > V_d > C_s$ (C_s is the sound speed). The significance of this will be discussed later in connection with specific instability mechanisms.

2. *Parallel bias (↑↑)*

Toroidal magnetic field profiles corresponding to the initial parallel bias configuration are shown in Fig. 7(a). Initially, a broad sheath structure is discernible which propagates inward at an average speed of about 1.5×10^7 cm/sec. A steepening of the piston is barely observable, however, and the field diffuses rapidly into the plasma by about 0.9 μsec. The diamagnetic character of the profiles is considerably diminished at 1.0 μsec, although profiles at later times [Fig. 7(b)] again show diamagnetic behavior, probably due to a radial oscillation of the plasma column.

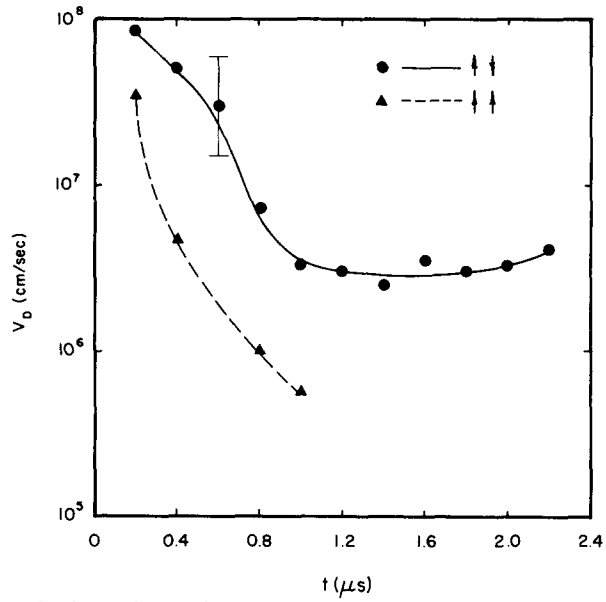

FIG. 6. Relative drift velocity, $V_d = V_i - V_e$, as a function of time estimated from magnetic field profiles, for antiparallel and parallel bias cases.

The diffusive nature of the parallel bias field profiles has previously been observed in the Maryland fast linear theta pinch[32] and implies enhanced resistivity in the current sheath. From the observed sheath width of

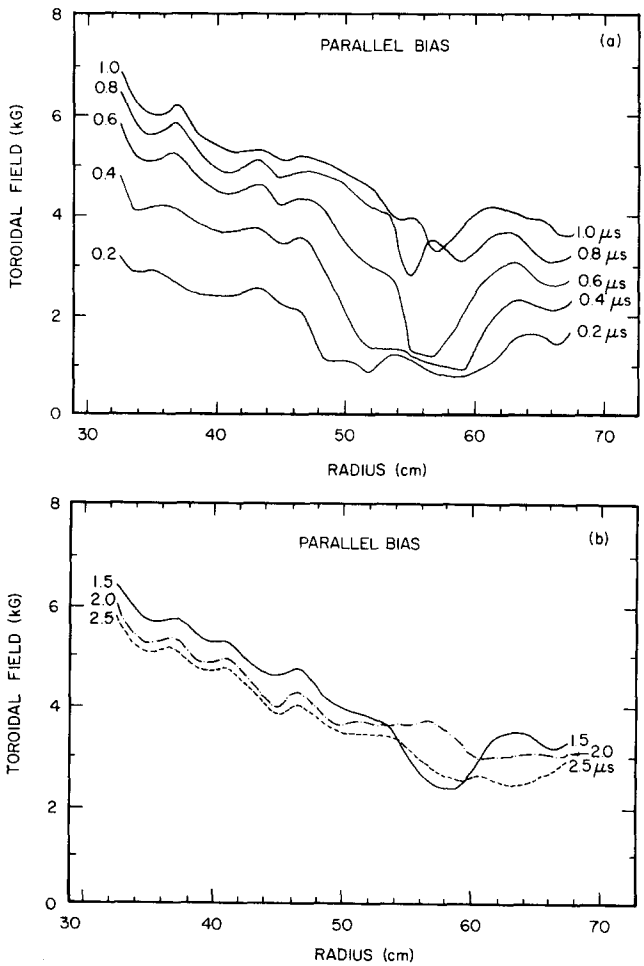

FIG. 7. Toroidal magnetic field profiles for the parallel bias case: (a) profiles for 0.2 μsec to 1.0 μsec, (b) profiles at 1.5, 2.0, and 2.5 μsec.

9 cm at 0.5 μsec [~$6(c/\omega_{pi})$ at 5×10^{14} cm^{-3}], we estimate a resistivity $\eta^{\uparrow\uparrow}\approx 2\times10^{-12}$ sec and a poloidal current density of 8×10^{11} SA/cm^2. The corresponding drift velocities $V_d\approx J/ne$, for this parallel mode, are shown as the dashed curve in Fig. 6. As in the previous case, the drift velocity is estimated from the field profiles and sheath densities obtained from laser interferometry. The relatively low drift velocities observed with parallel bias fields have important consequences in connection with possible microinstabilities in the sheath region.

B. Ion heating

An important question addressed by toroidal theta pinch experiments is whether the various ion heating and thermalization mechanisms based on microinstabilities remain as effective when the electron energy is confined. As a first approximation, we can obtain some knowledge of the ion heating from the speed of the magnetic piston. Ions which are carried along with the magnetic piston will have an energy of $E_i=\frac{1}{2}m_i v_p^2$, where v_p is the magnetic piston speed. A fraction of the ions may be reflected at twice the piston speed by the electrostatic potential associated with the magnetic sheath. This directed ion energy may eventually thermalize as the piston converges to the axis, either by repeated bouncing or by some collisionless mechanism[33] leading to an ion temperature given by

$$\tfrac{1}{2}m_i v_p^2 \le kT_i \le \tfrac{1}{2}m_i(2v_p)^2 . \tag{6}$$

For deuterium ions moving at an average piston speed $v_p=1.4\times10^7$ cm/sec, we obtain an ion temperature given by 200 eV $\le kT_i \le$ 800 eV, which holds for the antiparallel bias case and for the early implosion phase ($t<0.8$ μsec) of the parallel bias case. Previous results on the linear theta pinch[15] and numerical modeling indicate fewer reflected ions in the parallel bias mode and less thermalization of piston ions. This estimate, obviously, does not include any additional ion heating that may take place.

Ion temperatures were also estimated from the observed neutron yields. Typical scintillator-photomultiplier signals of neutron emission for the antiparallel and parallel bias cases are shown in Fig. 8. In both cases, the neutrons are emitted in several bursts lasting about 100 nsec. For convenience of measurement, these time-resolved neutron bursts are passively integrated (RC = 50 nsec) and from the pulse areas we obtain $N(\uparrow\downarrow)=1.2\times10^6$ neutrons per shot for the antiparallel case and $N(\uparrow\uparrow)=3.6\times10^4$ neutrons per shot for the parallel case. The neutron yields were calculated assuming an emitting volume given by $V=(2\pi R_0)(\pi r^2)$, with $R_0=56$ cm and $r=6$ cm for the antiparallel case and $R_0=56$ cm and $r=7.5$ cm for the parallel case. The emission times were taken as 0.4 and 0.25 μsec for the antiparallel and parallel cases, respectively. These neutron yields correspond to a mean ion energy of 3 keV ($\uparrow\downarrow$) and 2 keV ($\uparrow\uparrow$) at $n_{e0}=2\times10^{14}$ cm^{-3} assuming a one-dimensional monoenergetic ion distribution. For a fully three-dimensional Maxwellian ion distribution at the same density, we would obtain 2 keV ($\uparrow\downarrow$) and 1 keV ($\uparrow\uparrow$), respectively. The assumption of a monoenergetic distribution may be realistic due to the directed nature of the ion energy during the early implosion. However, as noted earlier, this directed energy may eventually thermalize leading to a more isotropic distribution of ion energies. The ion energies derived from neutron yields are larger than the kinetic energies of ions that would be elastically reflected from the imploding piston (approximately 0.8 keV), probably indicating additional energization due to microinstabilities in the piston region, as observed in the University of Maryland small theta pinch.[34]

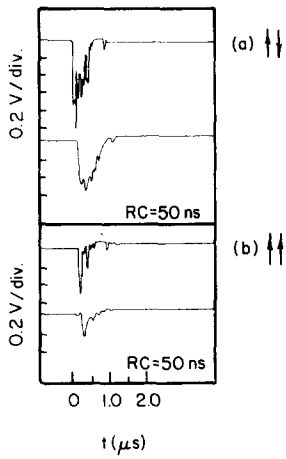

FIG. 8. Typical photomultiplier signals of neutron emission: (a) antiparallel bias, (b) parallel bias. Top trace in (a) and (b) are time resolved neutron pulses and bottom traces are integrated at RC = 50 nsec.

Further information concerning ion heating was obtained by spectroscopic observations on lines of impurity ions. The deuterium is very rapidly ionized in the compressed plasma, and thus its lines only originate from the cooler regions outside the plasma core. Carbon is a naturally occurring impurity, and the CIII line at 2297 Å and the CV lines near 2270 Å were studied in order to probe in the hot region of the plasma. An optical multichannel analyzer device was used that enabled complete spectra of these lines to be obtained at several spatial positions simultaneously. The optical setup is shown in Fig. 9. The size of the image in the plasma, determined by the size of the optical multichannel analyzer detector and the spectrometer slit width, was 8 cm by 0.01 cm. The long dimension was aligned along a major radius of the torus. The 8 cm long image could be divided up into smaller images and the spectrum from each measured separately using the two-dimensional mode of the optical multichannel analyzer. The reciprocal dispersion of the spectrometer

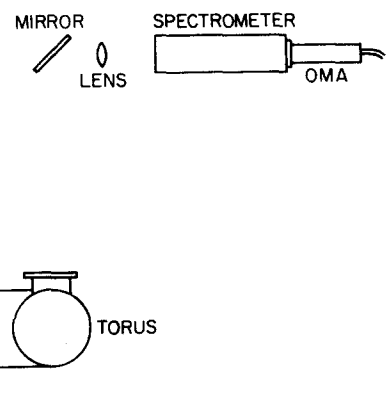

FIG. 9. Optical multichannel analyzer optical setup.

used was 6.9 Å/mm yielding a resolution of 0.17 Å/channel. For all of the data given below the optical multichannel analyzer was pulsed on for 250 nsec, so the spectra are integrated over that time period. The times given with the data are delays between the start of the main bank and the beginning of the 250 nsec period. The Stark broadening of the carbon lines is negligible for our conditions, so the line shape is entirely due to the Doppler effects corresponding to the velocity distribution of the ions and due to the instrumental broadening.

On some of the shots a magnetic probe was present which projects to, or near to, the center of the plasma. The presence of the probe had a substantial effect on the spectra obtained. This effect is described and explained below.

The spectra obtained in the antiparallel bias case indicate a relatively hot plasma as CV lines are present. Spectra at 1.1 μsec at three spatial positions are shown in Fig. 10. These data were taken with the magnetic probe inserted. The C III line at 2297 Å shows a complex shape on all three spectra indicating a directed velocity of the ions as well as thermal broadening.

The CV lines appear nearly Gaussian at $R = 59.6$ and $R = 58.0$, but at $R = 56.4$ each of them is split into two distinct components with a separation of 2.7 Å, corresponding to a velocity of 3.6×10^7 cm/sec. The split between the CIII components at $R = 56.4$ is 2.4 Å. For those shots with the magnetic probe inserted, a clear splitting of these lines into two components was observed on about 25% of the shots, and about 50% of the shots showed asymmetric lines or lines with non-Gaussian shapes indicating a nonresolved splitting of the two lines. In order to arrive at a temperature from the shape of these lines, only those spectra were used that showed a good fit to a Gaussian or to a sum of two Gaussians. No split or asymmetric lines were seen with the magnetic probe out of the plasma.

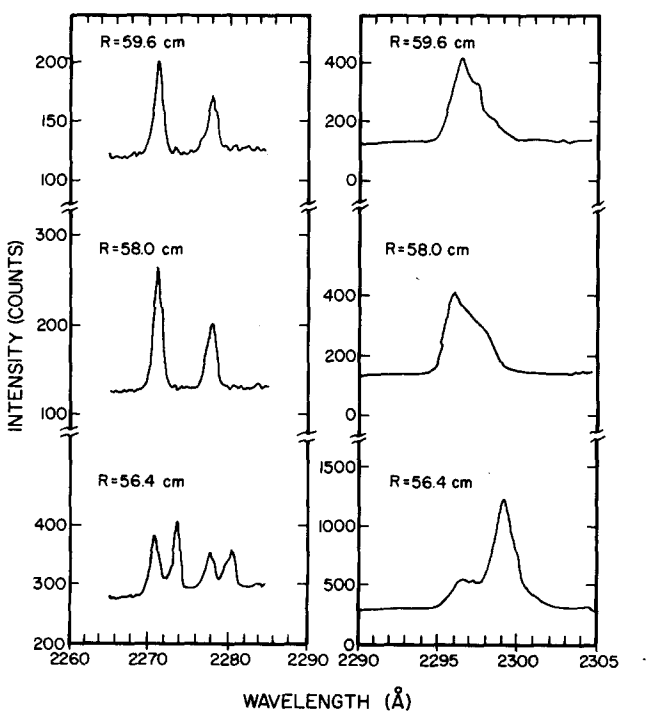

FIG. 10 Spectra of CV and CIII lines at three radial positions.

The ion temperatures obtained from the width of the CIII lines are shown in Fig. 11. The temperatures measured without the probe present were considerably lower than those with it. A possible explanation of this is that the probe is a source of carbon at the center of the plasma. Carbon knocked off the walls of the vacuum vessel by the plasma may not have time to diffuse into the center of the plasma. Thus, without the probe the carbon ions may only be present in the cool periphery of the plasma, while with the probe inserted, carbon is present in the hot central plasma. This is supported by the fact that the CV lines without the probe were much weaker than with the probe, while the C III lines were approximately the same intensity in both cases.

For those lines that showed a clear splitting, a plot of the separation of the components vs their average temperature is shown in Fig. 12 for data from C III and CV. There appears to be a correlation between the two quantities, higher temperatures occurring on those shots that show a greater splitting.

In the parallel bias case CIII was observed, but CV was absent, indicating a lower electron temperature than in the antiparallel case. The CIII line was never observed to split into two components as was sometimes observed in the antiparallel case. However, the C III line was very broad in those shots in which the magnetic probe was present, and we believe this was due to an unresolved splitting of the line. Figure 13 shows the ion temperature vs time at several spatial positions for shots without the magnetic probe. It is seen that the temperature rises more rapidly than in the antiparallel case but decreases rapidly at about 1 μsec, while in the antiparallel case the temperature is still increasing at that time.

The temperature of the deuterium ions is not necessarily equal to the temperature of the carbon ions since

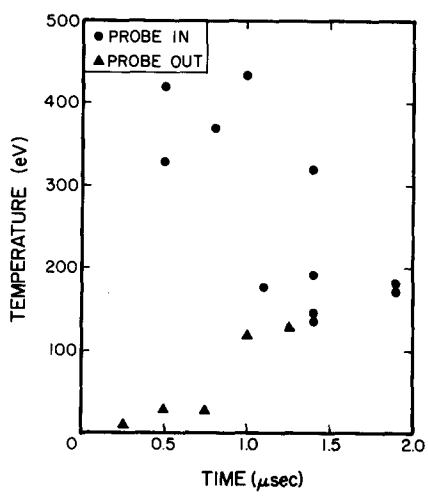

FIG. 11. Carbon ion temperatures with antiparallel bias field vs time, with and without magnetic probe present.

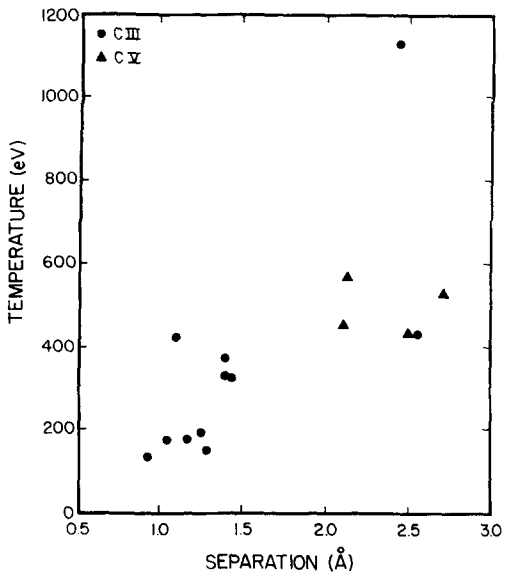

FIG. 12. Separation of Doppler split components of carbon lines vs temperatures obtained from Doppler broadening.

the heating mechanism for the ions may be charge and/or mass dependent. However, Coulomb collisions are effective in equalizing their temperatures. For example, for a CV temperature of 500 eV, a deuterium ion temperature of 50 eV, and a deuteriuum density of 2×10^{15} cm^{-3}, the thermal equilibration time would be approximately 0.24 μsec. One mechanism for ion heating is the reflection of the ions off the magnetic piston formed during the implosion as has been observed spectroscopically in linear theta pinches.[34,35] This could explain the large shifts seen in the carbon lines. If the ions, including the deuterium, are heated primarily by this mechanism, then they would all be accelerated to approximately the same velocity, and the kinetic energy of the different species of ions would be proportional to their mass. Thus, the deuterium ions would have one sixth the energy of the carbon ions or about 60 eV. However, the deuterium temperature deduced from the neutron measurements given here gave a much higher temperature than this. It is possible that the observed neutrons are due to a high energy ion distribution, whereas the spectroscopic measurements are more indicative of the bulk ions. Such two-temperature ion distributions have been observed in other high-voltage theta pinch devices.[15,36] The fact that the large shifts in the carbon lines did not occur on every shot argues against the simple explanation due to reflection off the piston. Also, the large shifts were seen on a few shots at times of 1.4 μsec and later after the implosion was over. A possible explanation for the Doppler shifts is a magnetohydrodynamic instability causing rapid plasma motion. The instability could be sensitive to small changes in the initial conditions or in the compression so that it occurs only infrequently. From Fig. 10 it can be seen that the disturbance in the plasma can be highly localized since there is strong mass motion at $R=56.4$ and none observable at the other positions for the C V lines. The C III lines show a complex structure at all three spatial positions. The C III and C V lines probably originate in different regions with the C V present in the hot core of the plasma and the C III lines at larger radius. Thus, a localized instability could affect the C III and the C V lines differently. The velocity of the spectroscopically observed mass motion is comparable to the characteristic velocities of the plasma. The sound speed at $T_e=200$ eV is 1.0×10^7 cm/sec, and the Alfvén velocity at a deuterium density of 10^{15} cm^{-3} and $B=3000$ G is 1.5×10^7 cm/sec.

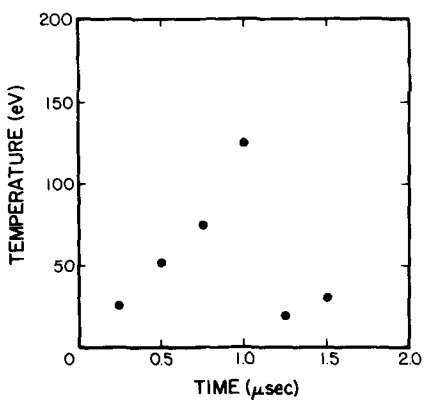

FIG. 13. Carbon ion temperatures with parallel bias field versus time without magnetic probe.

C. Electron heating

Plasma and target x-ray emission measurements were used to study the electron heating in both the antiparallel and parallel bias cases. Therefore, direct comparisons of the heating results can be made. The target x-ray diagnostic is most sensitive to electrons with mean energies in the range from 7–11 keV, while the plasma x-ray diagnostic has operated with peak sensitivity in the range from 0.9–1.5 keV. Thus, it was possible under the experimental conditions to resolve a hot (nonthermal) and the bulk (thermal) electron component.

1. Antiparallel bias

Radial profiles (in the horizontal midplane) of the target x-ray intensity attenuated by a 25 μm Al filter are shown in Fig. 14 for various times after initiation of the coil current. During the implosion [Fig. 14(a)], we observe a broad intensity peak propagating inward with an instantaneous position that corresponds approximately to the position of the current sheath. This intensity peak, corresponding to the inside magnetic sheath, coalesces with the (outside) intensity peak at $R\approx62$ cm by 0.8 μsec and forms a stationary structure at $R\approx58$–60 cm. For times greater than 1.0 μsec [Fig. 14(b)], a stationary double peak structure is evident which roughly coincides with the position of the current sheath. Peak target x-ray intensity occurs at about 1.2 μsec. Subsequently, the plasma expands slightly and the x-ray intensity decreases, dropping to about 10% of the peak by 3 μsec.

The electron temperature corresponding to the target x-ray emission was obtained from intensity ratios through 25 and 250 μm Al filters. The target x-ray temperatures averaged over the outside sheath pos-

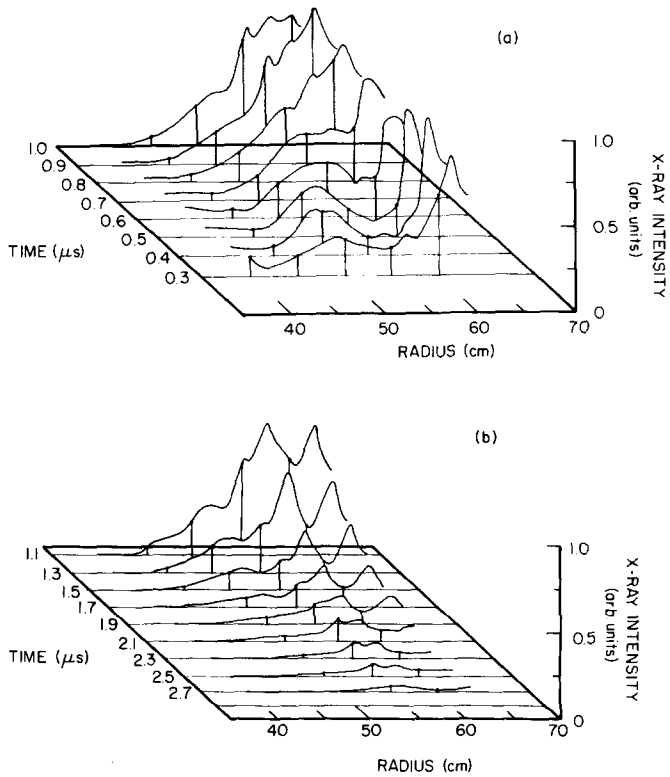

FIG. 14. Radial profiles of antiparallel bias target x-ray intensity through 25 μ Al filters: (a) $t = 0.3$–1.0 μsec; (b) $t = 1.1$–2.7 μsec.

itions ($R = 60$–64 cm) are plotted in Fig. 15 (solid line) as a function of time. The measured temperatures are in the range from 2–7 keV. The density of electrons at the measured temperature was estimated from the absolute target x-ray intensity and is shown as the dashed line. Evidently, these hot electron temperatures (denoted by T_{eh}) correspond to a small fraction (< 1%) of the bulk electron density ($n_e \approx 10^{15}$ cm^{-3}).

Beryllium filters (12.5 and 50 μm) were inserted into the detection system and the target was removed in an attempt to observe the bremsstrahlung x-ray emission from the bulk electrons. Estimates of the contribution from the hot electrons indicated that it would be possible to resolve the emission from the bulk component. Profiles of the soft x-ray emission as a function of viewing direction show a dynamic structure which is consistent with the emission expected from an imploding plasma column. For $1.0 \lesssim t \lesssim 1.5$ μsec, a well localized emission is observed indicating a hot plasma occupying the outer half of the torus. This is in agreement with the plasma dynamics as inferred from the magnetic field profiles.

Electron temperatures derived from intensity ratios of soft x-ray emission are shown in Fig. 16 for viewing directions of 0°, 20°, and 40° ($\theta = 0$: radially out, $\theta = 180$: radially in). The typical standard deviation from shot-to-shot was 25 eV with a maximum standard deviation of 70 eV. The measured temperatures are in the range of 150–300 eV. The absolute intensity of the soft x-ray emission is consistent with calculations of bremsstrahlung and recombination radiation on 2%

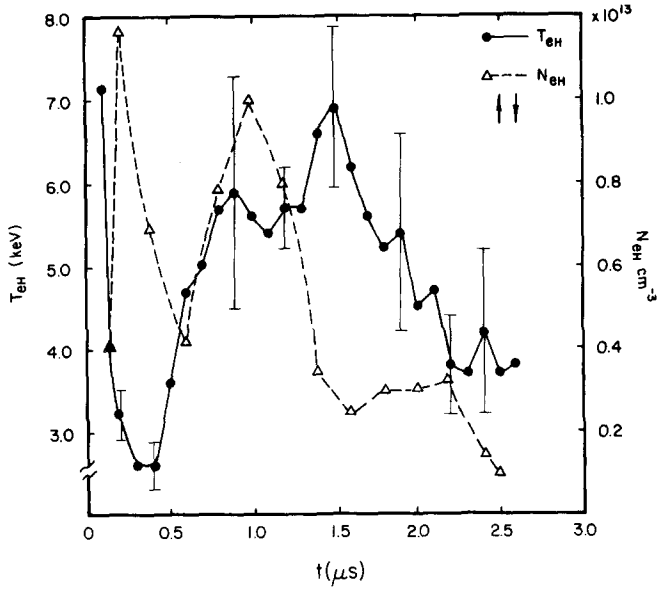

FIG. 15. Electron temperature and density derived from target x-ray measurements averaged over outside sheath positions ($R = 60$–64 cm) for antiparallel bias condition.

oxygen impurities at the measured electron density ($\approx 2 \times 10^{15}$ cm^{-3}). Thus, we conclude that the soft x-ray derived temperatures do indeed reflect the bulk electron population. At the earliest times during the implosion ($t < 0.2$ μsec), the density is low and the plasma x-ray emission is probably dominated by the hot electron distribution. By 0.5 μsec the plasma emission is clearly due to the bulk electrons and the temperature increases up to about 1.5 μsec. The time history of the bulk electron temperature is probably determined by several factors including the observation geometry and the increasing influx of relatively cold electrons as ionization becomes complete. For the purposes of comparison, the bulk electron pressure $n_e T_e(\theta = 0°)$ and hot electron pressure $n_{eh} T_{eh}$ (averaged over outside sheath positions)

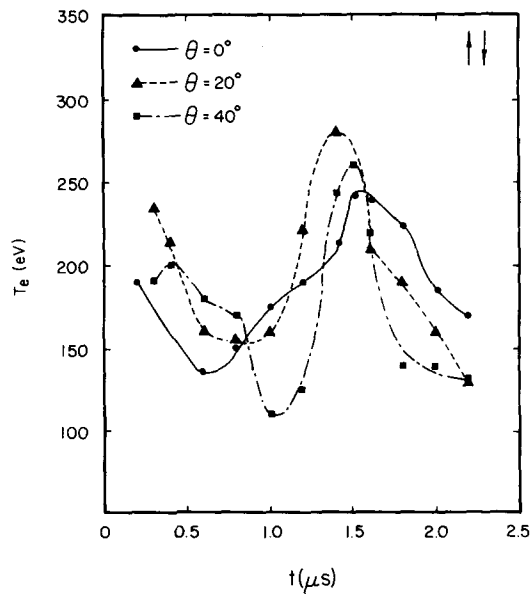

FIG. 16. Electron temperature derived from soft x-ray intensity ratios for viewing angles of 0°, 20°, and 40° for antiparallel bias case.

are shown in Fig. 17. The bulk electron pressure is computed using the electron density (estimated from laser interferometry) appropriate for the magnetic sheath region. During the early implosion phase ($t<0.5$ μsec) most of the energy density resides in the hot component, but for $t \gtrsim 0.5$ μsec the bulk distribution dominates the electron energy content.

2. Parallel bias

Target x-ray emission was observed in the parallel bias case but with intensities which were about 10 times smaller than in the previous antiparallel case. A radial target scan indicated that significant x-ray emission occurs only in the range $R = 50-54$ cm, which roughly coincides with the position of the broad inside current sheath The target x-ray intensity corresponding to the outside current sheath was almost a factor of 10 smaller than the intensity in the range $R = 50-54$ cm. This may be related to the observation that the electron density is a maximum in the outer sheath region.

The (target x-ray deduced) electron temperature averaged over the positions of peak intensity ($R = 50-54$ cm) is shown in Fig. 18. The rather large error bars are indicative of the poor shot-to-shot reproducibility of the x-ray emission in the parallel bias case. The temperature rises to about 3 keV by 0.8 μsec and rapidly decreases with the decay of the diamagnetic currents in the plasma as seen from the magnetic field profiles. The electron densities corresponding to the measured temperatures are also shown in Fig. 18. The peak density (7×10^{13} cm^{-3}) represents about 3% of the bulk electrons. During the first microsecond, the hot electron energy density is about an order of magnitude less than the energy density observed in the antiparallel case.

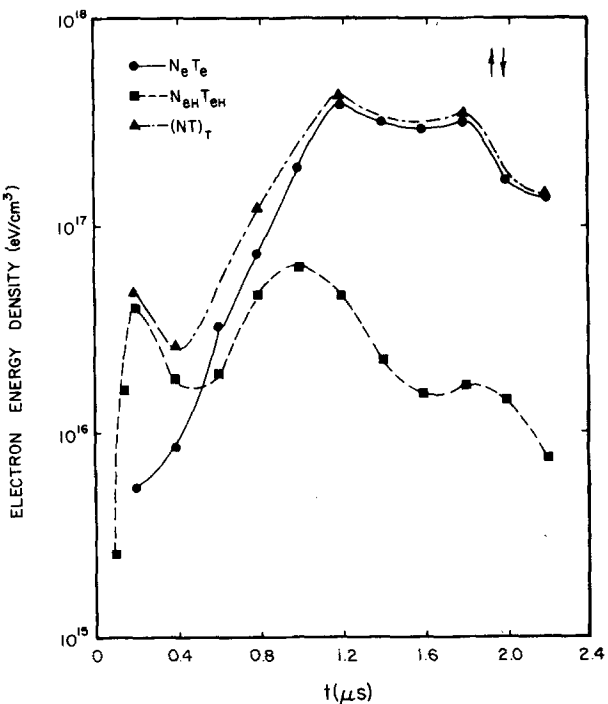

FIG. 17. Hot and bulk electron energy densities (eV/cm^3) for antiparallel bias case.

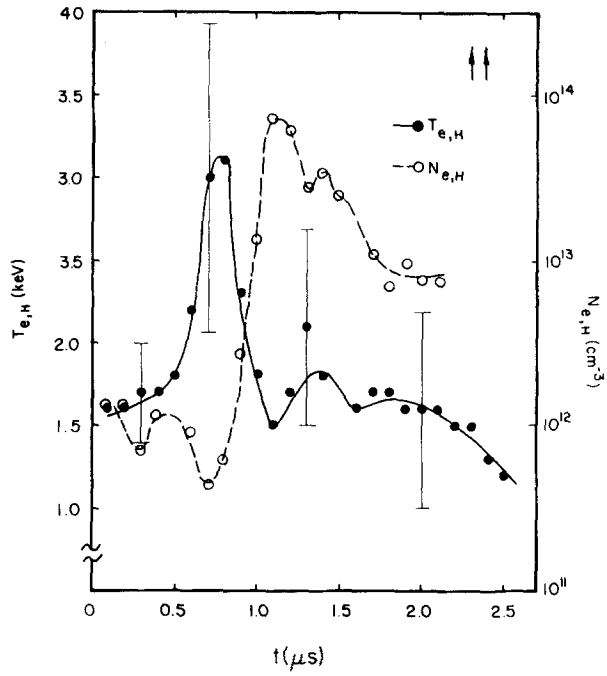

FIG. 18. Electron temperature and density, derived from target x-ray emission, averaged over positions of peak intensity ($R = 50-54$ cm) for parallel bias condition.

Observations of relatively weak, soft x-ray plasma emission indicate that the bulk electron temperature in the parallel case is less than 100 eV. This is consistent with the spectroscopic observations of impurity carbon ions.

The effects of the magnetic probe on the impurity spectral line intensities has already been discussed. We have also attempted to determine what effects, if any, the x-ray target produced. In this regard the following observations were made. First, the neutron yields were unaffected either by the presence of the x-ray target or magnetic probe or both. Second, the x-ray target had no effect on the spectral line profiles. Third, the soft x-ray emission was unaffected by the magnetic probe. These observations are probably connected with the fact that the x-ray target was 180° away (in the toroidal sense) from the location of the spectroscopic measurements and 120° from the magnetic probe. In contrast the magnetic probe measurements and spectroscopy were performed in adjacent ports (60° apart). The substantial effect of the magnetic probe on the spectroscopic observations is probably related to the close proximity of the measurements.

V. DISCUSSION

In the antiparallel case the target and plasma x-ray measurements indicate a two-temperature electron distribution with a hot electron tail at $T_{eh} \approx 3-7$ keV, which is a small fraction (~0.5%) of the bulk distribution that is characterized by $T_e \approx 200$ eV. We point out that electrons on the tail of a thermal distribution could not be responsible for producing the target x rays since their proportion for $T_e = 200$ eV would be less than 10^{-5}.

The hot-electron component is probably due to acce-

leration of electrons in the poloidal electric field near the field reversal region. A quasi-linear treatment[37] of the response of a one-dimensional plasma to an applied electric field E_0 showed that the electrons are accelerated to approximately one-half of the free-streaming value, i.e., $\dot{v}_e(t) = eE_{ot}/2m$. Using a simple model of the measured toroidal field profiles and integrating Maxwell's curl **E** equation, we estimate that $E_\theta \approx 3.8$ SV/cm(1.1 kV/cm). Electron acceleration in this field would result in an electron energy of 7.5 keV in 5 nsec. Early in the implosion when the driving voltage is highest and the peripheral density low, this mechanism would be most efficient in accelerating electrons. Continued electron acceleration in the imploding neutral layer may continually drive superthermal tails by quasi-linear plateau formation which occurs on the time scale of ω_{pe}^{-1} (Ref. 38) Recent theoretical work has indicated that superthermal electron tails may be produced by strong turbulence stabilization of beam-plasma instabilities.[39] This nonlinear stabilization process transfers fluctuating field energy from wavelengths resonant with the beam to shorter wavelengths which can interact with background electrons to form superthermal tails. Similar parameteric instability processes have been proposed to explain high-energy electron tails observed in laser-plasma interactions.[40]

The bulk electron heating in the antiparallel case can be discussed within the context of the various cross-field current driven microinstabilities responsible for the observed heating in comparable linear experiments. A consideration of the growth conditions of the various microinstabilities and the relative magnitude of the drift velocity as compared with the relevant plasma parameters indicates that the ion-acoustic and lower hybrid drift instabilities are most likely responsible for the observed bulk electron heating. The ion-acoustic instability is important when the relative drift speed exceeds the acoustic velocity C_s and $T_e \gg T_i$. Since $v_d > C_s$, and assuming $T_e \gg T_i$ in the sheath region, we expect the ion acoustic instability to be operative in our experimental regime. The lower hybrid drift instability is driven by cross-field currents in the presence of gradients in density, temperature, and magnetic field. This instability differs from the ion acoustic instability in that it can grow in regions where $T_i \leq T_e$. We have estimated the growth rates and electron heating levels (eV/cm^3) based on these instabilities using values of plasma parameters appropriate to the current sheath region. The fluctuation levels for these instabilities were taken from the results of computer simulation studies. Over a fairly wide parameter range both the ion-acoustic and lower-hybrid-drift instabilities can grow to sufficient levels on the experimental time scale. The calculated electron heating rates and anomalous resistivities are in good agreement with the electron heating measurements and the magnetic field profiles.

To directly observe the effects of the microturbulence, measurements were made of the spectrum of far infrared emission near the electron plasma frequency and its first harmonic.[41] A nonthermal spectrum was observed covering a wavelength range from approximately 0.63–0.28 mm with a peak intensity that is at least two or three orders of magnitude greater than that expected from a thermal plasma.

In the parallel bias case, a high-energy electron distribution was observed in the range from 1–3 keV with the highest electron energies corresponding to 1–4% of the bulk distribution. This hot electron component has not been observed in similar linear theta pinch experiments operating with parallel bias fields. Apparently, the elimination of end losses allows higher electron temperatures than have otherwise been possible. With parallel bias fields we do not expect electron acceleration in the current sheaths as in the antiparallel case where a neutral layer exists. The electrons are essentially magnetized everywhere, which should result in an **E×B** drift inward in response to the driving field.

We might expect that the enhanced level of electrostatic fluctuations in the plasma would lead to rapid cross-field diffusion. The time scale for diffusion of hot electrons out of the current sheath may be estimated by computing an across field diffusion coefficient $D_\perp$ based on an effective collision frequency ν_{eff} derived from microinstability theory, i.e.,

$$D_\perp = \nu_{eff} T_{eh}/m_e \omega_{ce}^2, \tag{7}$$

where T_{eh} is the hot electron temperature and ω_{ce} is the electron cyclotron frequency.[42] Since in the antiparallel bias case the electrons may diffuse into a region of relatively weak magnetic field, we find that $D_\perp(\uparrow\downarrow) \approx 10^2 D_\perp(\uparrow\uparrow)$. The diffusion time scale, Δt can be estimated from

$$\Delta t \approx (\Delta x)^2/2D_\perp, \tag{8}$$

when (Δx) is taken as the characteristic sheath width, resulting in $\Delta t(\uparrow\downarrow) \approx 0.1$ μsec and $\Delta t(\uparrow\uparrow) \approx 50$ μsec. This simple estimate indicates that the diffusion of hot electrons in the antiparallel case occurs on a relatively short time scale. The hot electrons may diffuse out of the current sheath and into the central core of plasma where some of the nonthermal energy may be converted to bulk electron energy. In the parallel bias case this diffusion process would not be observed on the experimental time scale.

The ion-heating results presented here are comparable to the results of similar linear theta pinch experiments. In the antiparallel case the bulk ion temperature is $T_i \approx 100$–400 eV from spectroscopy, while neutron emission measurements gave $T_{in} \approx 2$–3 keV. In the parallel case $T_i \approx 50$–150 eV and $T_{in} \approx 1$–2 keV. In both cases the neutrons are emitted during the first 0.5 μsec, whereas the bulk ion temperature peaks at about 1 μsec. The neutron derived temperature (T_{in}) is probably more indicative of ions which have acquired large directed velocities in the early implosion phase. These ions may eventually thermalize with background ions leading to a somewhat lower bulk temperature and a decrease in the neutron emission. A more definitive interpretation of the ion heating would require spatially resolved measurements, although these results are qualitatively similar to the results of the linear case.

In contrast the electron heating measurements now indicate $T_e \approx T_i$, whereas in open ended systems $T_e/T_i < 1$. In particular linear theta pinches are characterized by a core of hot ions and relatively cold electrons ($T_i \gg T_e$) surrounded by a hot electron sheath.[4,5,43] The average temperature of these hot electrons which are associated with the current sheath is usually less than the bulk ion temperature. In the toroidal case the temperature of the hot sheath electrons (T_{eh}) is greater than or comparable to the bulk ion temperature and these hot electrons persist even beyond the implosion phase. In the parallel bias case a population of hot electrons was observed although no significant bulk electron heating was observed. In the Maryland fast linear theta pinch, x-ray emission corresponding to energetic electrons was only observed in the field null region in the antiparallel case. We also note that the results of the toroidal theta pinch are consistent with electron and ion heating in a high-voltage belt pinch.[44]

The comparison of the linear and toroidal theta pinch experiments is complicated by the fact that the toroidal field has an intrinsic $1/R$ radial dependence and a small poloidal field is present to prevent the outward drift of the initial plasma. The $1/R$ dependence of the toroidal field leads to an asymmetric implosion due to the different values of the applied magnetic field at the inner and outer edge of the torus. Although an asymmetric implosion may affect the radial dependence of the plasma parameters, we believe that the comparison of the relative average ion and electron temperatures in the linear and toroidal cases to be valid.

The effect of the poloidal field due to the induced toroidal current is to introduce a relatively weak magnetic shear. The influence of magnetic shear on the microinstability properties of the magnetic sheath region has been investigated analytically[45] and numerically.[46,47] Magnetic shear was shown to stabilize the lower hybrid drift instability when the length scale characterizing the magnetic shear is $L_s < L_n(a_i/L_n + L_n/a_i)$, where $L_n \equiv d(\ln n)/dx$ is the density gradient scale length and a_i is the ion gyroradius. For typical parameters of our experiment we expect $L_s > L_n$ due to the relatively small value of the poloidal field. However, in the antiparallel case the effect of the poloidal field in the vicinity of the field null may be important. In this region, however, the relative drift velocity v_d is high and we expect $T_e > T_i$, so that the dominant microinstability process is probably the ion-acoustic instability.

In other experiments where the lower hybrid drift instability is expected to be important, the stabilizing effects of magnetic shear have not been observed. In Tormac V anomalous penetration of the applied toroidal field is observed in a plasma with an initial parallel bias toroidal field and strong shear.[48] In computer simulations of the University of Maryland paramagnetic spheromak experiment large resistivity and anomalous ion heating rates are observed in a high density pinch possessing strong magnetic shear.[49] A detailed study of the macroscopic behavior of the toroidal pinch including the evolution of the poloidal flux surfaces has been the subject of a separate investigation.[50]

VI. SUMMARY AND CONCLUSIONS

Rapid heating of electrons and ions has been observed in a high-voltage toroidal theta pinch with bias fields either parallel or antiparallel to the fast rising toroidal field. In both cases superthermal electron populations were observed corresponding to a small fraction of the total number of thermal electrons, but with the same energy density as the bulk electrons. Effective bulk heating was observed with antiparallel bias fields with heating rates in good agreement with microinstability predictions. The effects of the microturbulence were also observed as an enhanced bremsstrahlung emission near ω_{pe}. The hot electron distribution observed in the antiparallel case is related to the presence of a neutral layer in which electron acceleration and beam relaxation lead to superthermal tails. The high energy electrons observed with parallel bias fields are presumably due to a stochastic acceleration mechanism, since free streaming is prohibited by the magnetic field. Rapid cross-field diffusion of the hot electrons out of the current sheath appears as a significant transport mechanism in the antiparallel case. However, rapid diffusion of the magnetic field in the parallel case prohibits diffusion of hot electrons on the experimental timescale.

In contrast to the results of linear theta pinch experiments the elimination of electron energy losses along open field lines has permitted higher electron temperatures and now $T_e \sim T_i$. The ion heating is about the same and we can conclude that the microinstability processes[9] remain effective in an experiment where rapid end losses are eliminated. More effective electron and ion heating was observed with antiparallel bias field which are similar to observations on the Maryland fast theta pinch.[4] Finally, on some shots rapid plasma motion has been observed, probably due to a localized magnetohydrodynamic instability.

ACKNOWLEDGMENTS

We are grateful to Kenneth R. Diller and David L. Miller for their excellent technical support in the construction and operation of this experiment and to Eugene Day for his expertise with the data acquisition system.

This work was supported by the U.S. Department of Energy. One of the authors (R. L. M.) was partially supported by a grant from the National Science Foundation. Some of the material in this article is part of a thesis submitted by R. L. Merlino in partial fulfillment of the requirements for the degree of Doctor of Philosophy at the University of Maryland.

[1] A. C. Kolb, in *Proceedings of the Second United Nations Conference on the Peaceful Uses of Atomic Energy*, Geneva, 1958 (United Nations, Geneva, 1958), Vol. 31, p. 328.
[2] D. A. Tidman and N. A. Krall, *Shock Waves in Collisionless Plasmas* (Wiley, New York, 1971), p. 138.
[3] R. Z. Sagdeev, in *Reviews of Plasma Physics* (Consultants Bureau, New York, 1966), Vol. 4, p. 75.

[4]W. D. Davis, A. W. DeSilva, W. F. Dove, H. R. Griem, N. A. Krall, and P. C. Liewer, in *Plasma Physics and Controlled Nuclear Fusion Research*, Madison, Wisconsin, 1971 (International Atomic Energy Agency, Vienna, Austria, 1972), Vol. III, p. 289.
[5]R. Chodura, C. T. Dum, M. Keilhacker, M. Kornherr, H. Niedermeyer, R. Protz, F. Soldner, and K. H. Steuer, in *Plasma Physics and Controlled Nuclear Fusion Research*, Tokyo, Japan, 1974 (International Atomic Energy Agency, Vienna, Austria, 1975), Vol. III, p. 397.
[6]S. Gold, A. W. DeSilva, and J. D. Huba, Phys. Fluids 23, 1132 (1980).
[7]R. K. Linford, W. T. Armstrong, D. A. Platts, and E. G. Sherwood, in *Plasma Physics and Controlled Nuclear Fusion Research*, Innsbruck, Austria, 1978 (International Atomic Energy Agency, Vienna, Austria, 1979), Vol. II, p. 447.
[8]G. C. Goldenbaum, J. H. Irby, Y. P. Chong, and G. W. Hart, Phys. Rev. Lett. 44, 393 (1980).
[9]R. C. Davidson and N. A. Krall, Nucl. Fusion 17, 1313 (1977).
[10]P. C. Liewer and N. A. Krall, Phys. Fluids **16**, 1953 (1963).
[11]P. Bogen, K. J. Dietz, K. H. Dippel, E. Hintz, K. Hothker, F. Siemsen, and G. Zeyer, in *Plasma Physics and Controlled Nuclear Fusion Research*, Madison, Wisconsin, 1971 (International Atomic Energy Agency, Vienna, 1972), Vol. III, p. 277.
[12]R. J. Commisso and H. R. Griem, Phys. Fluids 20, 44 (1977).
[13]M. Z. Caponi and N. A. Krall, Phys. Fluids 18, 699 (1975).
[14]A. W. DeSilva, W. F. Dove, I. J. Spalding, and G. C. Goldenbaum, Phys. Fluids 14, 42 (1971).
[15]T. T. Chiang and A. W. DeSilva, Phys. Fluids 21, 1053 (1978).
[16]E. Oktay, Phys. Fluids 17, 2261 (1974).
[17]R. A. Hess and H. R. Griem, Phys. Fluids 18, 1056 (1975).
[18]J. H. Irby, J. F. Drake, and H. R. Griem, Phys. Rev. Lett. 42, 228 (1979).
[19]Y. G. Chen, Phys. Rev. Lett. 37, 703 (1976).
[20]Y. G. Chen, C. Chin Fatt, Y. P. Chong, A. W. DeSilva, G. C. Goldenbaum, H. R. Griem, R. A. Hess, R. L. Merlino, and D. P. Murphy, Phys. Rev. Lett. 38, 1400 (1977).
[21]D. Markins, Y. G. Chen, C. Chin-Fatt, and A. W. DiSilva, in *Proceedings of the First IEEE International Pulsed Power Conference*, Lubbock, Texas, 1976, edited by M. Kristiansen (IEEE, New York, 1977), paper IIC-3.
[22]G. Lehner, in *Reactions Under Plasma Conditions*, edited by M. Venugopalan (Wiley, New York, 1971), Vol. II, p. 509.
[23]H. R. Griem, *Plasma Spectroscopy* (McGraw–Hill, New York, 1964), p. 285.
[24]J. H. Adlam and I. C. Taylor, Culham Laboratory Report CLM-R81, Culham Laboratory, Abington, Berkshire (1968).
[25]S. M. Hamberger, J. Jancarik, L. E. Sharp, D. A. Aldroft, and A. Wetherell, in *Plasma Physics and Controlled Nuclear Fusion Research*, Madison, Wisconsin, 1971 (International Atomic Energy Agency, Vienna, 1972), Vol. II, p. 37.
[26]R. D. Bengston, K. W. Gentle, J. Jancarik, S. S. Medley, P. Nielsen, and P. Phillips, Phys. Fluids 18, 710 (1975).
[27]V. F. Aleksin, V. A. Suprunenko, E. A. Sukhomlin, and N. I. Reva, Zh. Tekh. Fiz. 36, 620 (1966) [Sov. Phys.-Tech. Phys. 11, 465 (1966)].
[28]N. A. Dyson, Proc. Phys. Soc. 73, 924 (1959).
[29]J. H. Sparrow and C. E. Dick, in *Proceedings at the Fourth Conference on the Scientific and Industrial Application of Small Accelerators*, edited by J. F. Duggan and J. A. Martin, IEEE, New York (North Texas State University, 1976), p. 195.
[30]C. E. Dick, A. C. Luca, J. W. Motz, R. C. Placious, and J. H. Sparrow, J. Appl. Phys. 44, 815 (1973).
[31]J. Jancarik and P. T. Snowden, Phys. Rev. Lett. 40, 1376 (1978).
[32]E. Oktay, A. W. DeSilva, P. C. Liewer, Y. G. Chen, H. R Griem, R. Hess, and N. A. Krall, in *Plasma Physics and Controlled Nuclear Fusion Research* (International Atomic Energy Agency, Vienna, Austria, 1975), Vol. III, p. 365.
[33]R. C. Davidson and J. M. Ogden, Phys. Fluids 18, 1045 (1975).
[34]R. J. Commisso and H. R. Griem, Phys. Rev. Lett. 36, 1038 (1976).
[35]W. D. Davis, Phys. Fluids 15, 2383 (1972).
[36]K. Hothker, Nucl. Fusion 16, 253 (1976).
[37]S. Hamasaki, R. C. Davidson, and N. A. Krall, Phys. Fluids 14, 2385 (1971).
[38]A. A. Galeev and R. S. Sagdeev, in *Reviews of Plasma Physics* (Consultants Bureau, New York, 1979), Vol. 7, p. 72.
[39]H. L. Rowland, Phys. Fluids 23, 508 (1980).
[40]J. J. Thomson, R. J. Faehl, W. L. Kruer, and S. Bodner, Phys. Fluids 17, 973 (1979).
[41]C. Chin-Fatt, R. A. Hess, H. R. Griem, A. W. DeSilva, and G. C. Goldenbaum, Bull. Am. Phys. Soc. 25, 883 (1980).
[42]S. Ichimaru, *Basic Principles of Plasma Physics* (W. A. Benjamin, New York, 1973).
[43]P. Boger, K. J. Dietz, E. Hintz, K. Hothker, Y. T. Lie, and A. Pospieszcyzyk, in *Plasma Physics and Controlled Nuclear Fusion Research*, Tokyo, Japan, 1974 (International Atomic Energy Agency, Vienna, 1975), Vol. III, p. 349.
[44]F. Soldner, C. T. Dum, and K. H. Steuer, Phys. Rev. Lett 39, 194 (1977); F. Soldner, Phys. Fluids 21, 1036 (1978).
[45]N. A. Krall, Phys. Fluids 20, 311 (1977).
[46]N. T. Gladd, Y. Goren, C. S. Liu, and R. C. Davidson, Phys. Fluids 20, 1876 (1977).
[47]R. C. Davidson, N. T. Gladd, and Y. Goren, Phys. Fluids 21, 922 (1978).
[48]B. Feinberg, B. G. Vaucher, R. S. Shaw, and M. C. Vella, Phys. Fluids 24, 1342 (1981).
[49]A. G. Sgro and D. Winske, Phys. Fluids 24, 1156 (1981).
[50]D. P. Murphy, Ph.D. thesis, University of Maryland (1980).